PERGAMON

International Journal of Solids and Structures 36 (1999) 3709–3729

INTERNATIONAL JOURNAL OF SOLIDS and STRUCTURES

Induced damage by ellipsoidal cracks in an anisotropic medium

C. Barret, S. Baste*

LMP, C.N.R.S. UPRES A. 5469, Université Bordeaux 1, 33405 Talence Cédex, France

Received 29 January 1998; in revised form 18 May 1998

Abstract

This paper is concerned with an estimation of the effective elastic properties of an anisotropic body permeated by ellipsoidal cracks following the Eshelby's method. The classical integral expression of the *P*-tensor, the symmetrised derivative of the Green's tensor, is given for a 3D defined crack embedded in an anisotropic medium. The numerical evaluation of the *P*-tensor is validated with several limiting cases of simplified geometry cracks. The interest of a 3D representation of the cracks is shown with several applications: influence of the ellipticity and crack thickness aspect ratios, growing cracks. To conclude, a comparison between theoretical results and experimental data is done for the load-induced change of the compliance tensor for a damaged composite material.

1. Introduction

The overall elastic moduli of a solid are changed in the presence of microcracks. Eshelby (1957) has developed a remarkable method for the survey of heterogeneous inclusion in an infinite medium. This method has very often been used and extended to the anisotropic medium (Willis, 1964; Bhargava and Radhakrishna, 1964). These pioneer works are the basis of several methods developed to estimate the effective properties of a cracked solid. Among these methods, the Self-Consistent method (Hill, 1965; Budiansky and O'Connel, 1976; Hoenig, 1979; Hori and Nemat-Nasser, 1983) and the Differential Scheme (McLaughlin, 1977; Laws and Dvorak, 1987; Hashin, 1988; Deng and Nemat-Nasser, 1992) are the most used. They require the calculus of a fourth order tensor noted *P* that has been first defined by Hill (1965). Even if the integral formulation of *P* is well known, (Faivre, 1971; Laws, 1977a), the calculus of this tensor often requires numerical evaluations for arbitrary ellipticity of the inclusion. To avoid these numerical evaluations, the cases presented in the literature deal with geometry leading to analytical formulas. Firstly, one can consider the effect of spherical voids embedded in an isotropic body that leads to an analytical

* Corresponding author. Fax: 0033 556 846964; E-mail: baste@lmp.u-bordeaux.fr

0020–7683/99/$ - see front matter
PII: S0020–7683(98)00162–0

expression of the tensor P. Secondly, Laws (1977b) considers the ellipsoidal crack via the infinite elliptic cylinder in an anisotropic medium and obtains an approximated analytical expression of P. These approximations are useful to estimate effective elastic properties for two particular cases: concrete and composite laminates. Nevertheless, such a simplified geometry of a crack is no more efficient for other real material wherein cracks are really ellipsoidal.

By using an ultrasonic device, we know the variations of the stiffness tensor during the damage process for woven ceramic matrix composites (Audoin and Baste, 1994). In such a case, the crack length is limited by the material microstructure and the crack opening displacement is not negligible (He et al., 1994). Therefore it is necessary to evaluate the P-tensor for 3D defined cracks.

Our purpose is to present a numerical evaluation of P for several types of ellipsoids and materials without any approximation on the shape of inclusion. First, our numerical results are compared with classical approximations for both isotropic and anisotropic materials permitted by spherical or slit voids. Then, we pay attention to the effect of the crack's geometry. The prediction of effective elastic properties is presented for two types of problems, firstly growing cracks and finally a comparison between prediction and experimentation for a multiplication of cracks during a damage process.

2. Physical motivation

The global behaviour of CMCs is directly related to the ability of the material to crack (Evans and Zok, 1994). Transverse matrix microcracking is the basic mechanism of deformation in CMCs. The matrix microcracks are stopped and deviated in mode II by the 90° layers (Fig. 1). The mode II leads to fibre-matrix sliding. This sliding allows transverse crack opening displacement whose macroscopic result is the inelastic strain (He et al., 1994). As it represents a significant part of the total strain, the thickness of the cracks is no longer negligible.

The various scales of a woven composite strongly influence its behaviour. The extension of cracks is limited by the waviness of the bundles so that the infinite cylinder representation is no longer available. The various mechanisms of damage usually occur as follows: first, an inter-bundle

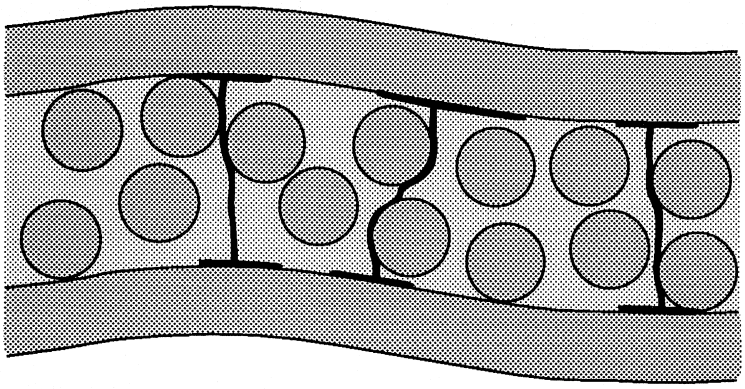

Fig. 1. Deviation in mode II of transverse cracks in a 2D composite.

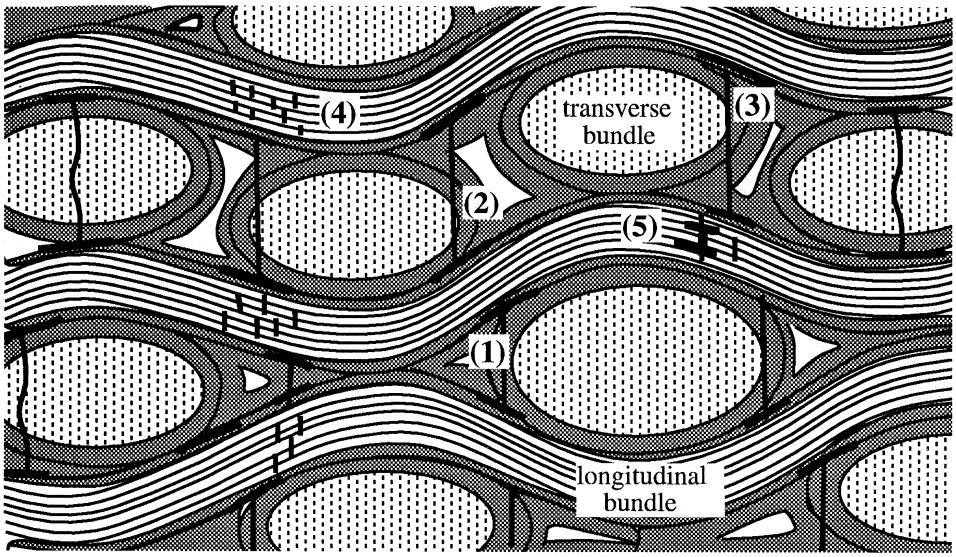

Fig. 2. Damage mechanisms in a woven 2D composite.

matrix cracking normal to the tensile axis (1) (Fig. 2) is observed, then it is deviated in mode II by the bundle–matrix interface and an array of longitudinal cracks (2), parallel to the tensile axis, appears. If the layers are prone to delamination, a third system has to be considered. It consists of a pattern of cracks parallel to the composite thickness (3). When the inter-bundle matrix is completely cracked, the mechanism comes to saturation. Then, the cracking spreads inside the longitudinal bundles (4). Inside the bundles, the fibres stop or deviate the intra-bundle cracks causing a fibre-matrix debonding (5).

Microcracking strongly modifies the elastic properties of the materials. There are two ways to study the damage mechanisms (Baste and Audoin, 1991). The macroscopic approach consists of measuring the internal structural changes by their effects on the mechanical response. The modification due to the damage process is defined as an additive tensor S_c and the compliance tensor of the damaged material, S becomes:

$$S = S_0 + S_c \tag{1}$$

where S_0 is the compliance tensor of the undamaged material.

The micromechanical approach consists of analysing the microscopic phenomena to predict the macroscopic behaviour. The microdefects are defined by their geometrical parameters a_i and their volume concentration c_c. A numerical or analytical treatment leads to the effective properties of the continuous equivalent damaged medium, (Wang et al., 1986):

$$S = S_0 + S_c(S_0, a_i, c_c). \tag{2}$$

3. Formulation of the problem

Let Ω, a representative volume of the material, be loaded by a uniform stress Σ. We have to calculate the average of the total strain E corresponding to Σ. Every type of inclusions embedded

in the material is regarded as a phase. Each phase i is characterised by its compliance tensor S_i and we have:

$$E = \sum_i \langle \varepsilon \rangle^i \quad \text{and} \quad \Sigma = \sum_i \langle \sigma \rangle^i \tag{3}$$

where $\langle \varepsilon \rangle^i$ and $\langle \sigma \rangle^i$ are the average strain and stress of the ith phase defined by:

$$\langle \varepsilon \rangle^i = S_i \langle \sigma \rangle^i. \tag{4}$$

Consider a solid with two phases: the undamaged material and an array of similar cracks. The first part of eqn (3) is then:

$$E = S_0 \Sigma + \varepsilon_{\text{fiss}} \tag{5}$$

where $S_0\Sigma$ and $\varepsilon_{\text{fiss}}$ are respectively the average strain of the undamaged material and of the cracks. Since the material remains elastic and homogeneous, $\varepsilon_{\text{fiss}}$ is linked to Σ by a local tensor B_n (Hill, 1965), then it follows:

$$E = (S_0 + B_n)\Sigma. \tag{6}$$

Equation (6) leads to the definition of the effective compliance tensor S_{eff}:

$$S_{\text{eff}} = S_0 + B_n. \tag{7}$$

The tensor B_n is representative of the change due to the cracks. It has been given by Laws et al. (1983) as:

$$B_n = c_c Q^{-1}, \tag{8}$$

where c_c is the volume concentration of cracks and Q^{-1} is the local compliance tensor for a single crack embedded in an infinite medium. Its definition stems from the works of Eshelby (1957) and Faivre (1971) and has been given by Laws (1977b):

$$Q^{-1} = (C - CPC)^{-1}, \tag{9}$$

where C is the stiffness tensor of the material and P is the symmetrised derivative of the Green's tensor. For an ellipsoidal crack defined by:

$$\frac{x_1^2}{a^2} + \frac{x_2^2}{c^2} + \frac{x_3^2}{b^2} \leqslant 1, \tag{10}$$

the integral expression of the fourth order tensor P is given by Faivre (1971):

$$P_{ijkl} = \frac{abc}{4\pi} \int_\Omega \frac{D_{ijkl}(\omega_n)}{(a^2\omega_1^2 + c^2\omega_2^2 + b^2\omega_3^2)^{3/2}} \, \mathrm{d}\Omega, \tag{11}$$

where Ω is the surface of the unit sphere centred at the origin of $(\omega_1, \omega_2, \omega_3)$ space. The fourth order tensor D is defined by:

$$D_{ijkl} = \omega_l \omega_j g_{ik} \tag{12}$$

and

$$g_{ik} = [C_{ijkl}\omega_j\omega_l]^{-1}_{(ik)}. \tag{13}$$

Obviously, P depends on both the stiffness of the material and the geometry of the cracks. Let two geometric parameters of the cracks be introduced: the crack ellipticity aspect ratio in the plane $(1,2)$: $\gamma = a/c$ and the crack thickness aspect ratio in the direction 3: $\delta = b/c$. By introducing these two parameters into eqn (11), it follows:

$$P_{ijkl} = \frac{\gamma\delta}{4\pi}\int_{\Omega}\frac{D_{ijkl}(\omega_n)}{(\gamma^2\omega_1^2+\omega_2^2+\delta^2\omega_3^2)^{3/2}}\mathrm{d}\Omega. \tag{14}$$

Let η be the number of cracks per unit volume then

$$c_c = \frac{4\pi}{3}\cdot abc\cdot\eta \quad \text{with} \quad \eta = \frac{1}{V_{\text{cell}}} = \frac{1}{2x_1\cdot 2x_2\cdot 2x_3}. \tag{15}$$

V_{cell} is the product of the distances between two cracks in the three normal directions of the space (Fig. 3). It represents the largest volume of material containing a single crack. By introducing f, the crack density parameter in the plane $(1,2)$:

$$f = \frac{4c^2}{2x_1\cdot 2x_2}$$

and β the crack density parameter in the third axis:

$$\beta = \frac{2c}{2x_3}, \tag{16}$$

c_c is defined with the two geometric parameters γ and δ by:

$$c_c = \frac{\pi}{6}\cdot f\cdot\gamma\cdot\beta\cdot\delta. \tag{17}$$

Equations (7) and (8) are the basic governing equations for the calculation of effective elastic

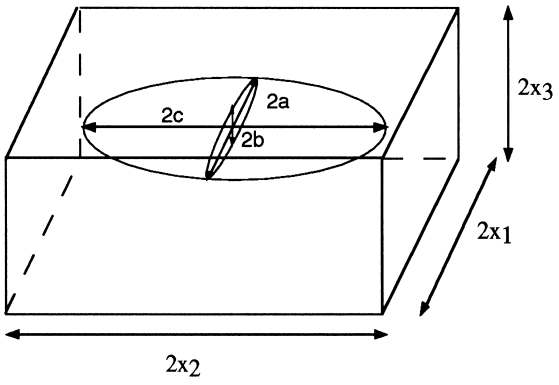

Fig. 3. Unit cell of a cracked body.

constants of bodies permeated by cracks. There are different approaches to resolve these equations. Firstly, one considers each crack as being embedded in the undamaged material (Mori and Tanaka, 1973), eqn (8) is then calculated with the initial stiffness tensor. Physically, the effect of the interaction between cracks is neglected and the change due to the cracks is obviously underestimated. On the contrary, in the self-consistent method, the crack sees itself as a single crack in the searched equivalent homogeneous medium. It attempts to account for inclusion interactions and eqn (7) is no longer explicit:

$$S_{\text{eff}} = S_0 + c_c Q^{-1}(S_{\text{eff}}^{-1}, P(S_{\text{eff}}^{-1})). \tag{18}$$

Equation (18) is less easy to calculate than eqn (7) with the Mori–Tanaka method but it leads to a more realistic evaluation of the effective compliance tensor.

The third method we will present is the self-consistent differential scheme. It is based on the notion of incremental construction of the damaged material by gradual addition of infinitesimal amounts of cracks. It leads to the resolution of a first order differential equation (MacLaughlin, 1977):

$$\frac{\mathrm{d}S_{\text{eff}}}{\mathrm{d}c_c} = \frac{1}{1-c_c} Q^{-1}(S_{\text{eff}}^{-1}, P(S_{\text{eff}}^{-1})), \tag{19}$$

with

$$S_{\text{eff}}(c_c = 0) = S_0. \tag{20}$$

This method is more efficient than the others for a porous medium or a large volume concentration of cracks but its physical interpretation is not easy (Zaoui, 1996), especially when several types of cracks are initiated simultaneously.

Figure 4 presents the comparison between the three methods for a multiplication of transverse cracks in an anisotropic medium. Only the three most influenced ones are plotted. The difference between the three methods is sensible only for large volume concentrations of cracks. In accordance with the results found in the literature, the Mori–Tanaka method gives the lower variation and the

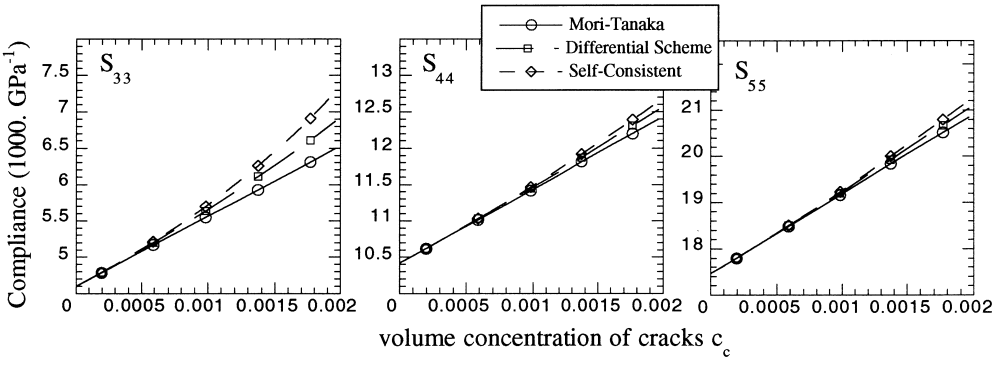

Fig. 4. Comparison of the effective elastic constants evaluation schemes. The three presented compliances as functions of the volume concentration of cracks are the most influenced ones.

self-consistent method gives the upper one. In order to obtain a realistic prediction for the effective elastic properties, we will use the self-consistent method in the following parts as the volume concentration of cracks does not reach large values in composite materials.

4. Evaluation of the *P*-tensor

Even if the integral eqn (14) is well known, its determination is a tricky problem for the calculus of the effective elastic properties. Moreover, the physical reality requires the determination of P_{ijkl} for ellipsoidal cracks and orthotropic medium. In such a case, eqn (14) cannot lead to analytical expressions. So, we have developed a numerical evaluation of the tensor P. The integrals are calculated by introducing spherical coordinates in eqn (14) with a 2D Simpson's method over the mesh of the rectangle $[0, \pi] * [0, 2\pi]$. The numerical results are compared with three classical models in Figs 5–7, in order to validate the calculus.

Firstly, we pay brief attention to an isotropic medium containing spherical cracks. Obviously, in such a case, the P-tensor is isotropic (Zhao et al., 1989). So it only requires the calculation of two integrals, P_{11} and P_{12} to determine the tensor P. As:

$$\gamma = \delta = 1, \tag{21}$$

eqn (14) falls in:

$$P_{ijkl} = \frac{1}{4\pi}\int_{\Omega} D_{ijkl}(\omega_n)\,\mathrm{d}\Omega, \tag{22}$$

with

$$D_{11} = \frac{\omega_1^4}{C_{11}} + \frac{(\omega_1^2 - \omega_1^4)}{C_{44}} \tag{23}$$

and

$$D_{12} = -\frac{\omega_1^2\omega_1^2}{C_{44}C_{11}}(C_{12} + C_{44}). \tag{24}$$

It leads to the final expressions:

$$P_{11} = \frac{1}{15} * \frac{7C_{44} + 2C_{12}}{C_{44}C_{11}} \tag{25}$$

and

$$P_{12} = -\frac{1}{15} * \frac{C_{44} + C_{12}}{C_{44}C_{11}}. \tag{26}$$

Secondly, the case of penny-shaped cracks is available in the literature (Laws, 1985). Analytical expressions of the P_{ijkl} are evaluated for an isotropic medium with a series expansion with respect to the thickness ratio δ. As $a = b$, it is possible to write eqn (14) with:

$$I(l,m,n) = \frac{\delta}{C_{11}C_{44}^2}\int_{-1}^{1} \frac{l+m\xi^2+n\xi^4}{(1-(1-\delta^2)\xi^2)^{3/2}}\mathrm{d}\xi. \tag{27}$$

The series expansion of the integral I with respect to δ up to order 2 leads to:

$$I(l,m,n) = \frac{2(l+m+n)}{C_{11}C_{44}^2} + \frac{\pi\delta}{C_{11}C_{44}^2}\left\{-3(l+m+n)+\frac{3l+m}{2}\right\}+O(\delta^2). \tag{28}$$

Equations (27) and (28) are similar to the expressions given by Laws (1985) for a transversely isotropic medium. For a penny-shaped crack embedded in an isotropic medium, as the plane (1, 2) remains isotropic, the evaluation of the tensor P is done by calculating P_{11}, P_{13}, P_{33}, P_{55} and P_{66}. We have:

$$\begin{aligned}
p_{11} &= \tfrac{1}{16}I(3C_{11}+C_{44}, \quad 0, \quad 0)\\
P_{13} &= \tfrac{1}{4}I(0, \quad -C_{44}(C_{11}-C_{44}), \quad C_{44}(C_{11}-C_{44}))\\
P_{33} &= \tfrac{1}{2}I(0, \quad C_{44}, \quad C_{11}-C_{44})\\
P_{55} &= \tfrac{1}{4}I(2C_{44}, \quad 4C_{11}-7C_{44}, \quad -4(C_{11}-C_{44}))\\
P_{66} &= \tfrac{1}{4}I(C_{11}+C_{44}, \quad -2C_{11}, \quad C_{11}-C_{44}).
\end{aligned} \tag{29}$$

The expressions given by Laws (1985) lead to the same results by considering an isotropic medium except for P_{55}. It may not have been printed properly.

Figure 5 is concerned with an isotropic material, a sample of epoxy resin elaborated by Ifremer and characterised by an ultrasonic method (Hosten et al., 1992), Table 1.

The results are plotted with respect to the thickness aspect ratio δ for circular cracks in the plane $(1,2)$, $\gamma = 1$. The components of P are evaluated with eqns (25) and (26) for the spherical inclusion. Equation (29) gives the P_{ij} for penny-shaped cracks. As they are defined for weak thicknesses, the results begin for $\delta = 0.1$. The results obtained with a numerical evaluation of eqn (14) lead to the same value than analytical expression for $\delta = 1$. Moreover, when δ tends to zero, the numerical results are similar to those obtained with the penny-shaped model. The differences observed for P_{33}, P_{44} and P_{55} are due to the three-dimensional representation of cracks, eqn (14). Indeed, however the numerical calculation takes the thickness into account, the penny-shaped model is a resolution of a 2D problem.

As most composite materials exhibit an orthotropic symmetry, we validate the numerical calculation of P also for this class of symmetry. Laws (1977b) has developed a model for slit cracks in an anisotropic medium by considering the crack as an infinite elliptic cylinder, $c \to \infty$, with a thickness aspect ratio $\varepsilon = b/a$ tending to zero. The non-zero components of P are (Laws, 1977b);

$$P_{11} = \varepsilon\frac{C_{33}+C_{55}(\alpha\beta)^{1/2}}{C_{11}C_{55}(\alpha^{1/2}+\beta^{1/2})\sqrt{\alpha\beta}}$$

$$P_{13} = -\varepsilon\frac{C_{13}+C_{55}(\alpha\beta)^{1/2}}{C_{11}C_{55}(\alpha^{1/2}+\beta^{1/2})\sqrt{\alpha\beta}}$$

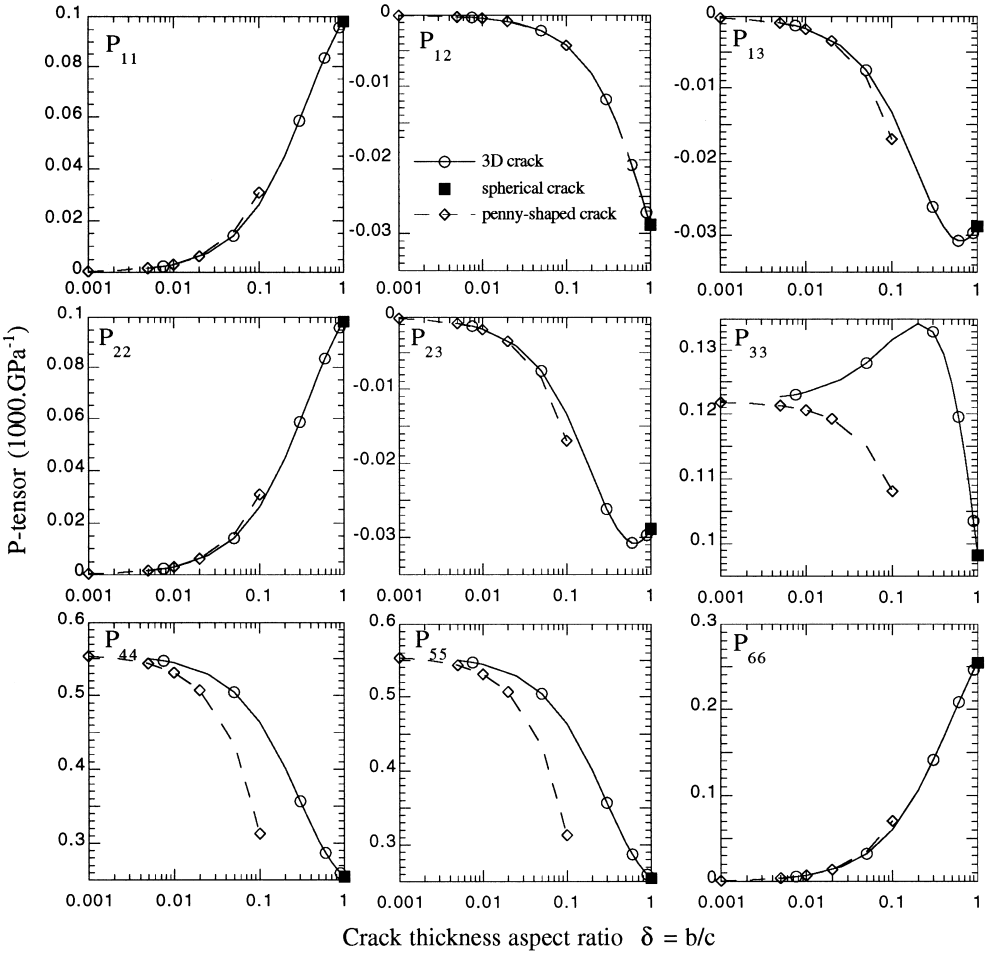

Fig. 5. The *P*-tensor as a function of the crack thickness aspect ratio for an isotropic medium.

Table 1
Stiffnesses of the isotropic medium

C_{ij} (Gpa)
$C_{11} = C_{22} = C_{33} = 8.2$
$C_{44} = C_{55} = C_{66} = 1.8$
$C_{12} = C_{13} = C_{23} = 4.6$

$$P_{33} = \frac{1}{4C_{33}} + \varepsilon \frac{C_{33} - C_{55}(\alpha + \beta + \alpha^{1/2}\beta^{1/2})}{C_{33}C_{55}\sqrt{\alpha\beta}(\alpha^{1/2} + \beta^{1/2})}$$

$$P_{44} = \frac{1}{C_{44}} - \varepsilon \frac{C_{66}^{1/2}}{C_{44}^{3/2}}$$

$$P_{55} = \frac{1}{C_{55}} - \varepsilon \frac{2(C_{11}C_{33} - C_{13}^2)}{C_{11}C_{55}(\alpha^{1/2} + \beta^{1/2})\sqrt{\alpha\beta}}$$

$$P_{66} = \varepsilon \frac{1}{(C_{44}C_{66})^{1/2}}, \tag{30}$$

where α and β are the roots of:

$$C_{11}C_{55}x^2 - (C_{11}C_{33} - C_{13}^2 - 2C_{13}C_{55})x + C_{33}C_{55} = 0. \tag{31}$$

In Figs 6 and 7, the numerical results are compared with eqn (30). As δ is no longer available for this model, P_{ij} are plotted with respect to the thickness aspect ratio defined by Laws, $\varepsilon = b/a$. We have considered two ceramic matrix composites, an orthotropic 1D SiC–SiC and a quasi-transversely isotropic 2D SiC–SiC in order to analyse the influence of the anisotropy on the variation of the P-tensor. The materials have been elaborated by the European Society of Propulsion (S.E.P.) and characterised (Table 2) by an ultrasonic method (Audoin and Baste, 1994).

The components of P are calculated for various ellipticity aspect ratios γ. Obviously, the weakest is γ, the nearest are the numerical results from the ones given by eqn (30). Whereas the infinite elliptic model leads to zero for the components in direction 2, numerical results show the influence of γ on these components. The comparison between the two models lead to the same remark about the influence of the thickness aspect ratio on P_{33} as with an isotropic medium. The P_{ij} are influenced not only by the geometric parameters but also by the anisotropy of the material considered. The observation is particularly relevant to the change of P_{33}. As C_{33} and C_{22} have different rates, the 1D SiC–SiC exhibits a strong anisotropy in direction 3 and the variations of γ do not change P_{33}. On the other hand, the 2D SiC–SiC is quasi transversely isotropic in the plane $(2, 3)$ and P_{33} is influenced by γ.

To conclude with the tensor P, one can say that the numerical evaluation of eqn (14) has been validated. Moreover, the differences between the simplified models and the numerical results illustrate the influence of the various parameters and the necessity of a three-dimensional approach in order to predict the changes due to a damage process in a best way.

5. Applications

The variations of the compliance tensor are directly related to c_c, eqn (8) and the spatial distribution of the cracks influences the evolution of the compliances, through f and β. Nevertheless the crack shape also modifies the evolution of S_{ij}. Figure 8 represents the variations of Q_{ij}^{-1} rather than S_{eff} to insist on the influence of γ and to avoid the effect of c_c. By considering the 2D SiC–SiC defined in Table 2 and a fictitious isotropic medium defined by the two compliances S_{33} and S_{44}

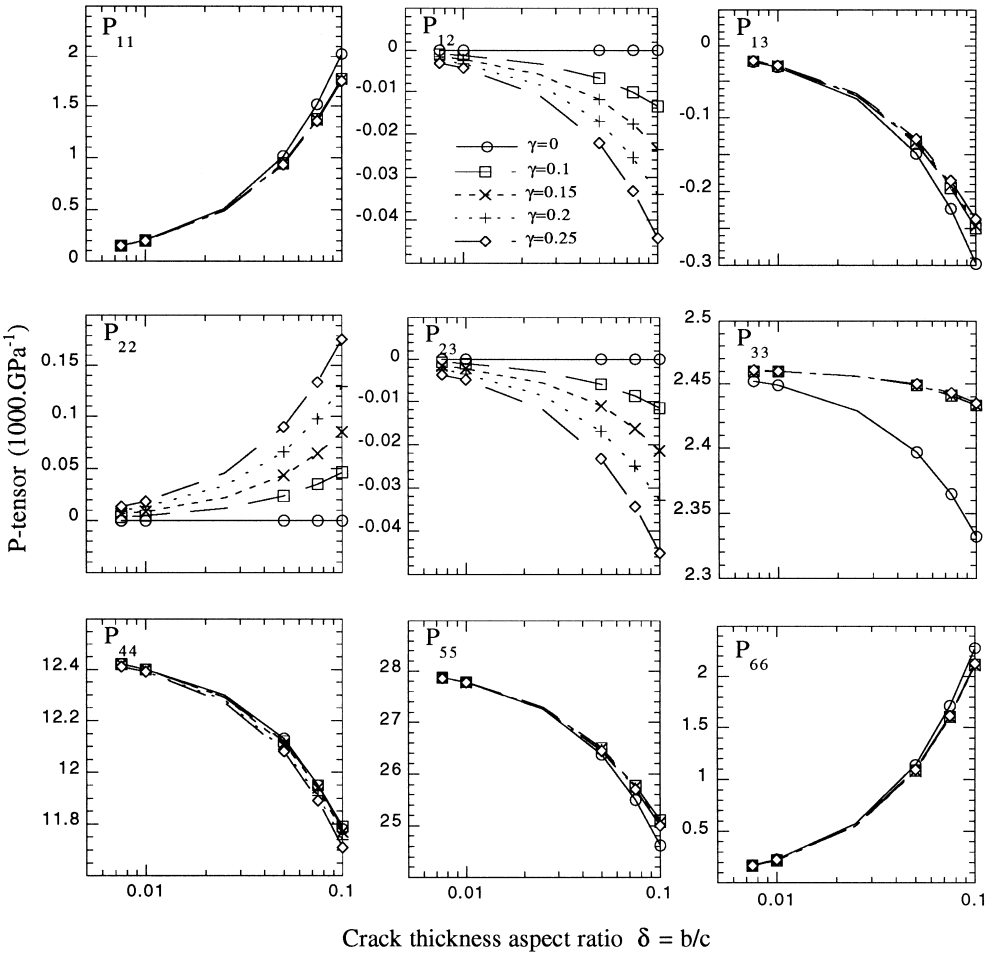

Fig. 6. The *P*-tensor as a function of the crack thickness aspect ratio and of the crack ellipticity aspect ratio γ for an orthotropic 1D SiC–SiC composite.

whose values are chosen equal to those of the composite, we have separated the geometric effect from the influence of the anisotropy. The results (Fig. 8) are given with respect to γ for several thickness ratios b/a. We have plotted only the most affected components Q_{33}^{-1}, Q_{44}^{-1} and Q_{55}^{-1}.

The weaker the ratio b/a is, the higher the influence of γ is. The thickness effect is therefore more important than the ellipticity in the plane (1, 2). Nevertheless, the ellipticity of the crack is of prime importance for thin cracks. It affects the three components in a different manner. As the evolution of γ is directly related to the value of c in the direction 2, Q_{44}^{-1} is more influenced by γ than the others. Indeed, for a fixed b/a, a decrease of γ induces a growth of the crack in direction 2 and so a more important change of the shear modulus of the plane (2, 3). The influence of γ on the Q_{33}^{-1} and Q_{55}^{-1} variation is the same for the two materials variations even if there are differences for Q_{55}^{-1} due to the definition of the fictitious isotropic material. On the other hand, concerning Q_{44}^{-1},

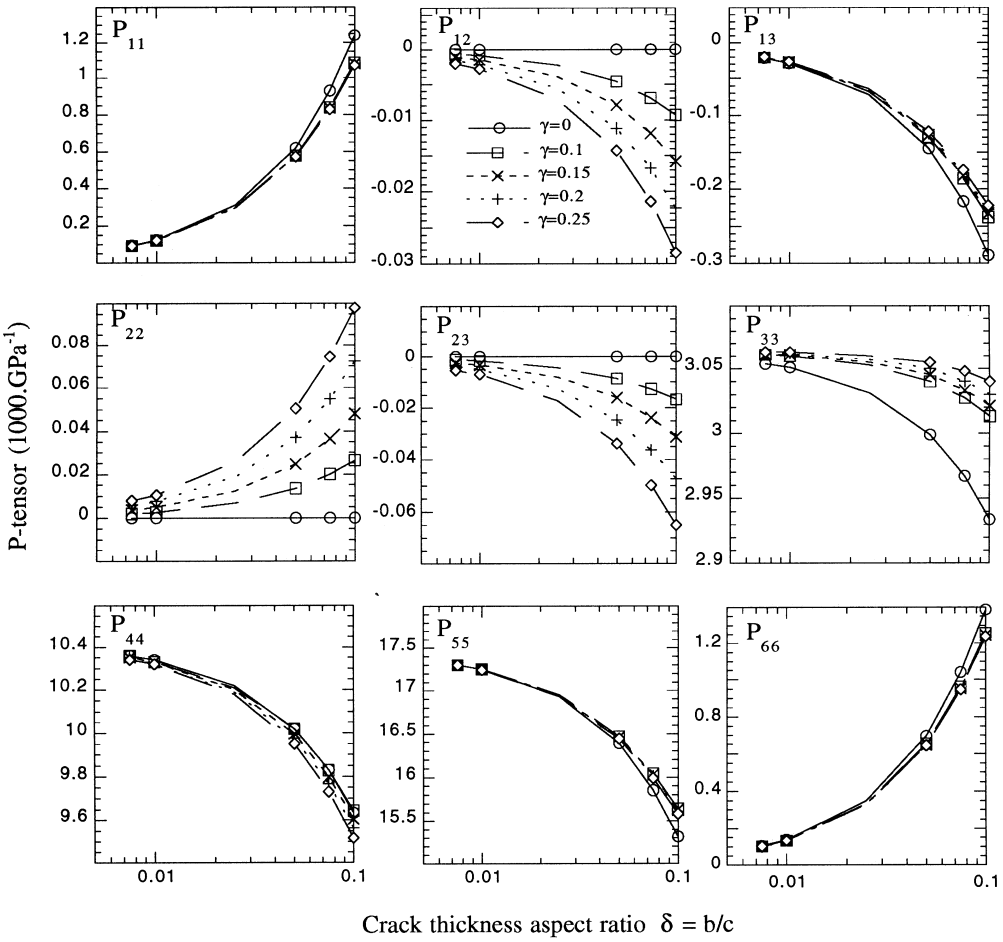

Fig. 7. The *P*-tensor as a function of the crack thickness aspect ratio and of the crack ellipticity aspect ratio γ for a quasi-transversely isotropic 2D SiC–SiC composite.

Table 2
Stiffness tensors of anisotropic media

	C_{ij} (GPa)								
	C_{11}	C_{12}	C_{13}	C_{22}	C_{23}	C_{33}	C_{44}	C_{55}	C_{66}
1D SiC–SiC	77	29	36	133	85	406	80	36	24
2D SiC–SiC	131	83	40	467	225	326	96	57	54

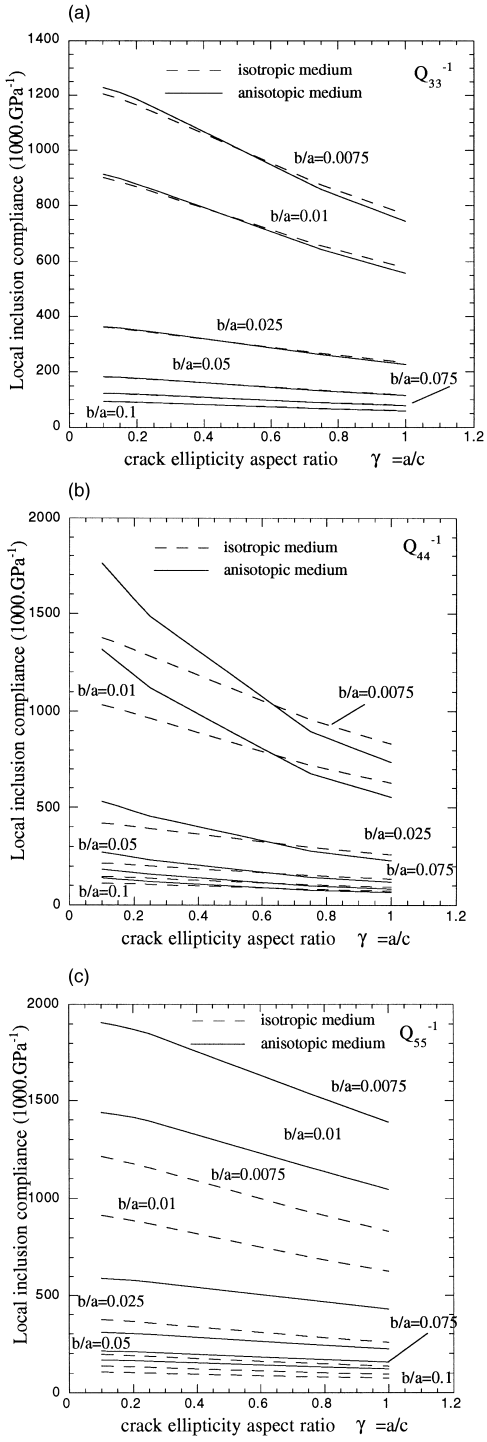

Fig. 8. The most influenced inclusion compliances as functions of the crack ellipticity aspect ratio $\gamma = b/c$ and as a function of the crack thickness aspect ratio $\varepsilon = b/a$.

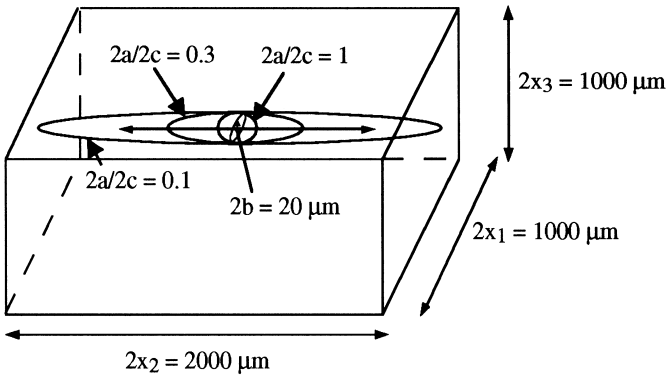

Fig. 9. A growing crack in the unit cell.

the influence of γ is more important for the anisotropic medium. Indeed, when $b/a = 0.0075$ for instance, Q_{44}^{-1} is twice as important for the 2D SiC–SiC as for the fictitious isotropic medium.

As the evaluation of the tensor P has been done for 3D cracks, the determination of the effective compliance tensor can be calculated for two categories of the problem. Firstly, the damage process can be represented by a multiplication of cracks with a fixed geometry. For instance, in a woven CMC, the cracks reach their size instantaneously as the bundles or the fibres limit their dimensions and the matrix microcracking leads to an increase in the number of cracks. Another damage process is defined at the microscopic scale by growing cracks. The fibre-matrix decohesion is an example of growing cracks with a fixed distribution. This problem has been treated by Deng and Nemat-Nasser (1992) for an isotropic medium and a 2D problem. The results we will present are concerned with 3D growing cracks in a 2D SiC–SiC (Table 2) and in the fictitious isotropic solid already defined. The dimensions of the unit cell of the material have been fixed, a and b have also been fixed, the crack is growing in direction 2. Figure 9 represents three steps of a crack propagating in the unit cell.

As $2c$ increases when the cracks are growing, it is necessary to calculate the effective compliance tensor for decreasing values of $\delta = b/c$ and $\gamma = a/c$. Figure 10 shows the change of δ and γ during the damage process with respect to $2c/2x_2$ where $2x_2$ is the distance between two cracks in direction 2. The fixed dimension of the crack in the other directions are $2a = 200$ μm and $2b = 20$ μm.

The effective compliance tensors are represented in Fig. 11 for the two materials with respect to $2c/2x_2$. The calculations are performed with the self-consistent method and the unit cell is defined in Fig. 9. The results are similar to the precedent application. Indeed, the anisotropy influences S_{44} more than the other components and the differences for S_{55} are due to the definition of the isotropic material. S_{33}, S_{44} and S_{55} remain the most influenced components. Obviously, the variations of S_{44} are more visible than the S_{55} ones as the cracks are growing in direction 2 and do not change in direction 1.

Whereas Fig. 11 deals with growing cracks, Fig. 3 is concerned with a multiplication of fixed geometry cracks but they have a similar change for the most influenced compliances S_{33}, S_{44} and

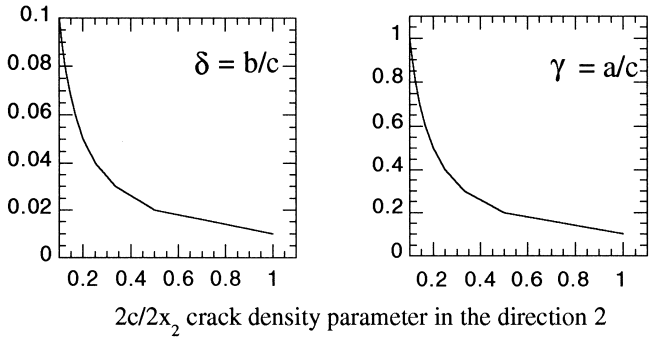

Fig. 10. Variations of the thickness and ellipticity aspect ratios for a growing crack.

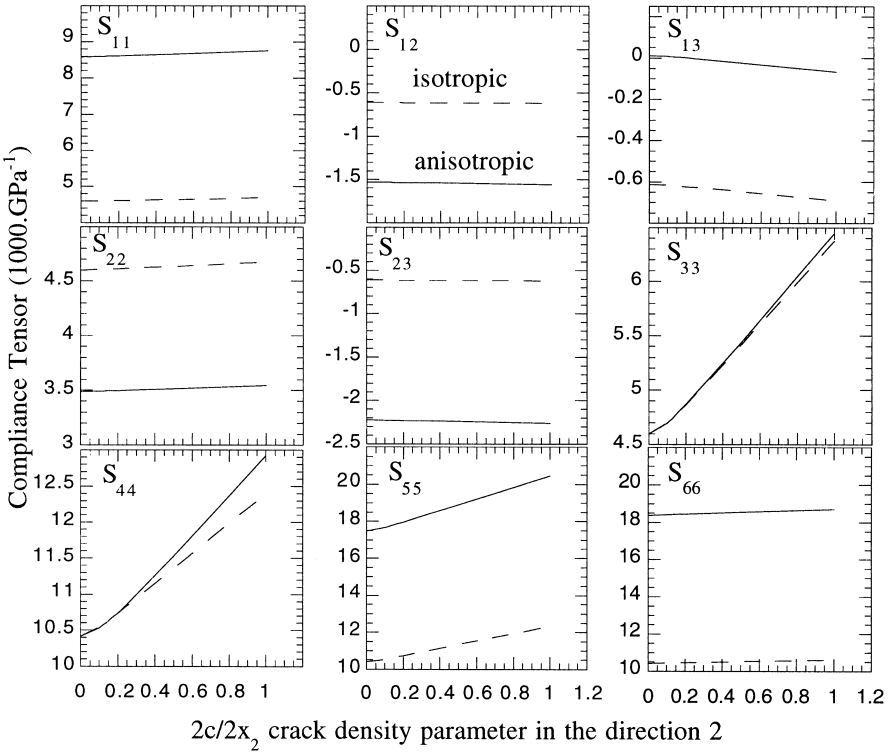

Fig. 11. Growing crack-induced variations of the compliance tensor.

S_{55}. This remark shows the importance of the material's microstructure. Indeed, the compliances variation indicates the orientation of microcracking but, without a morphological study of the material, it is impossible to know whether cracks are either growing or multiplying.

6. Comparison between experimental compliance changes and predictions on a 2D SiC–SiC composite

Let us consider a woven 2D SiC–SiC. This ceramic–ceramic composite is manufactured from preforms built up from multiple layers of Nicalon Silicon Carbide (SiC) fibre and the SiC matrix is added by a chemical vapour infiltration (CVI) process. As the matrix has a lower failure strain than the fibres, this composite exhibits rapidly a non linear behaviour mainly due to the matrix microcracking under tensile stress. Because of the woven nature of the composite, the plane (2, 3) is quasi isotropically transverse. The sample is a thin plate shaped, 3 mm in thickness and 2.7 g cm^{-3} in density. It was submitted to tensile stress in direction 3 parallel to the direction of one of the bundles.

An experimental device that couples an ultrasonic immersion tank with a tensile machine allows to know the changes of the complete stiffness and compliance tensor during a damage process for a composite material (Audoin and Baste, 1994).

Figure 12 shows the two scales of damage in the 2D SiC–SiC. The damage process starts at 80 MPa with a transverse matrix cracking at the inter-bundle scale. Then, longitudinal and interstacks cracking appear simultaneously at 90 MPa. The three arrays of cracks come to saturation at 120 MPa and the intra-bundle damage start (Figs 13 and 14). Whereas, the inter-bundle cracks are all slit cracks, the intra-bundle transverse matrix cracks are really ellipsoidal and the major axis is no longer in direction 2 but in direction 1 (Fig. 12).

The prediction of the equivalent compliance tensor has been done with a two-models self-consistent method. Indeed, the inter-bundle damage changes have been calculated with the infinite elliptic cylinder without thickness (Laws, 1977b). The equation for the equivalent compliance tensor is given by Laws et al. (1983) for an anisotropic medium with a longitudinal crack system:

$$S_{\text{eff}} = S_0 + \frac{\pi}{4}\beta_{\text{l}}\Lambda_{\text{l}}(S_{\text{eff}}^{-1}, S_0) \tag{32}$$

where β_{l} is the crack density parameter and Λ_{l} is given by:

$$\Lambda_{\text{l}}(S_{\text{eff}}^{-1}, S_0) = \lim_{\varepsilon \to 0} \varepsilon Q^{-1}(S_{\text{eff}}^{-1}, S_0). \tag{33}$$

Equation (32) is generalised for three crack systems by introducing β_{t} and β_{i} the crack density parameters for the 't' transverse and 'i' interstacks crack systems and Λ_{t} and Λ_{i} are obtained from the following index transformation

$$1 \to 1, 2 \to 3, 3 \to 2, 4 \to 4, 5 \to 6, 6 \to 5 \tag{34}$$

for the 't' transverse crack system; and

$$1 \to 2, 2 \to 1, 3 \to 3, 4 \to 5, 5 \to 4, 6 \to 6 \tag{35}$$

for the 'i' interstacks crack system. We have solved the implicit equation:

$$S_{\text{eff}} = S_0 + \frac{\pi}{4}\beta_{\text{t}}\Lambda_{\text{t}}(S_{\text{eff}}^{-1}, S_0) + \frac{\pi}{4}\beta_{\text{l}}\Lambda_{\text{l}}(S_{\text{eff}}^{-1}, S_0) + \frac{\pi}{4}\beta_{\text{i}}\Lambda_{\text{i}}(S_{\text{eff}}^{-1}, S_0) \tag{36}$$

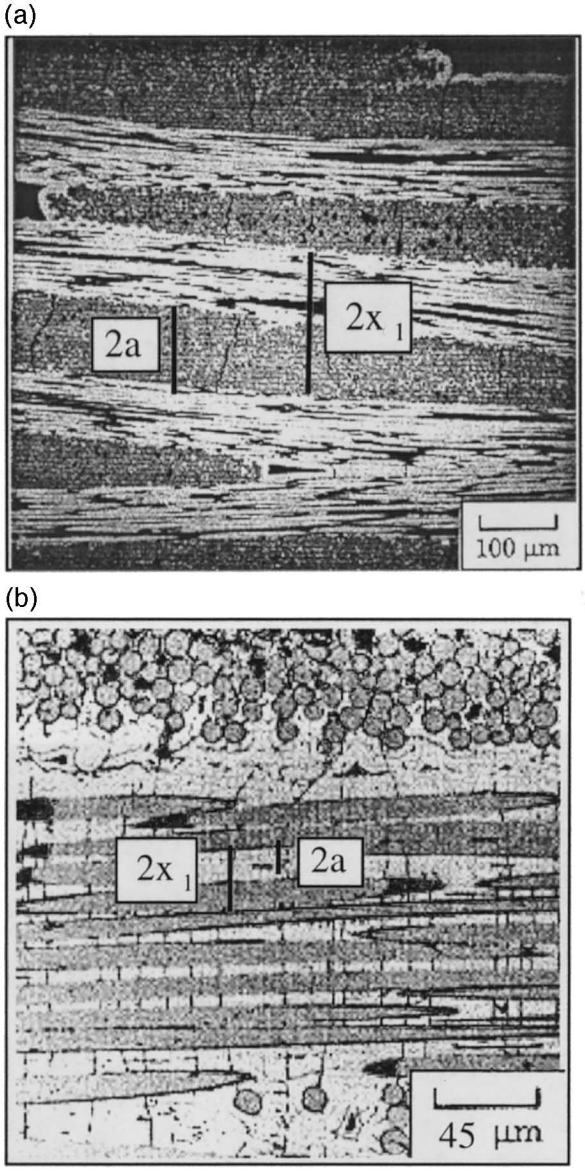

Fig. 12. Micrographs of the transverse cracks in a 2D SiC–siC. (a) Inter-bundle scale; (b) intra-bundle scale (Morvan and Baste, 1998).

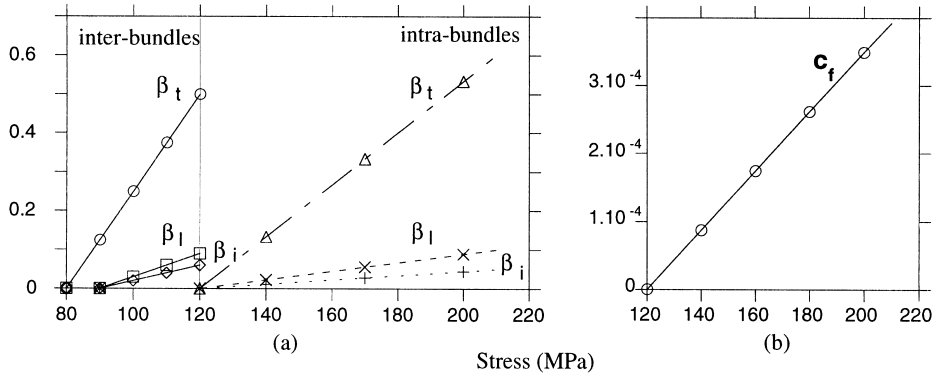

Fig. 13. Evolution of the crack distribution for the three arrays on two scales: (a) crack density parameters on two scales for the transverse crack β_t, the longitudinal crack β_l and the interstacks crack β_i; (b) volume concentration of transverse crack at the intra-bundle scale.

where β_t, β_l and β_i, the crack density parameters at the inter-bundle scale, are imposed with a linear increase (Fig. 13).

The model changes with the intra-bundle scale. As the geometry of the longitudinal and interstacks cracks remains the same, the infinite cylinder is still available for these arrays but the transverse cracks are then represented with real ellipsoids so $\pi/4\,\beta_t\Lambda_t(S_{\text{eff}}^{-1}, S_0)$ is changed by $c_c Q^{-1}$, eqn (8) where c_c is the volume concentration at the intra-bundle scale. The expression of the equivalent tensor is then:

$$S_{\text{eff}} = S' + c_c Q^{-1}(S_{\text{eff}}^{-1}, P(S_{\text{eff}}^{-1})) + \frac{\pi}{4}\beta_l\Lambda_l(S_{\text{eff}}^{-1}, S_0) + \frac{\pi}{4}\beta_i\Lambda_i(S_{\text{eff}}^{-1}, S_0) \tag{37}$$

where S' is the value of S_{eff} at 120 MPa calculated with eqn (36) and c_c, β_l and β_i, the crack density parameters at the intra-bundle scale, are imposed with a linear increase (Fig. 13). This method allows the prediction of the equivalent compliance tensor during the whole damage process (Fig. 14).

Figure 14 represents the variations of the 2D SiC–SiC compliance tensor during the load. Experimental values are given with their 90% confidence interval (Baste and Morvan, 1996) and predictions are plotted in a continuous line. The variations exhibit clearly three different domains. Compliances remain unchanged until the damage threshold. Then matrix microcracking begins and S_{33} sees an increase of more than 300% until saturation at 120 MPa. The variation of S_{33} becomes less visible as the matrix microcracking spreads inside the bundles. The same comments can be made for S_{22} and S_{11} although the variations are weaker. A good agreement is observed for the diagonal compliances especially for the first three ones. The differences observed for S_{44}, S_{55} and S_{66} are most probably due to the interaction between the different arrays of cracks that is not yet taken into account. This remark is also applicable to the extra-diagonal components.

7. Conclusion

A 3D representation of cracks has been developed. Even if it does not lead to analytical formulas, this method gives a more realistic approach to the physical phenomena. Indeed, it takes into

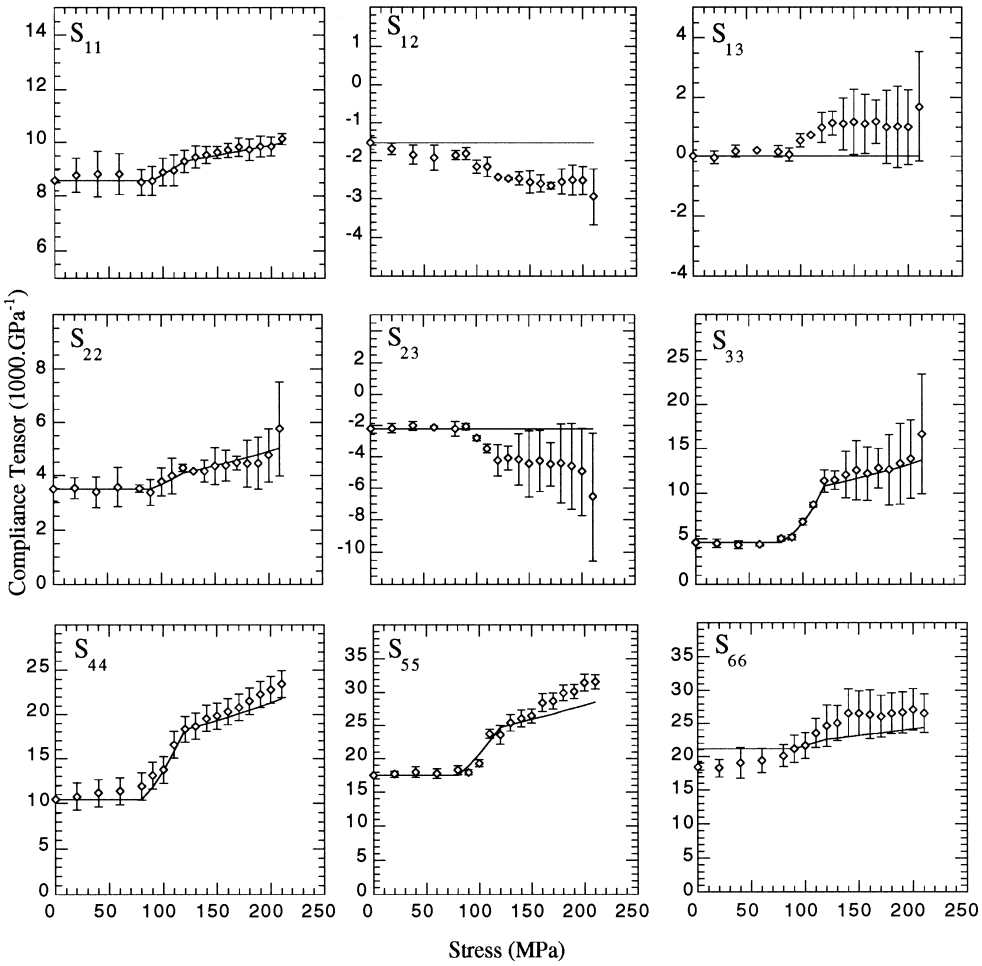

Fig. 14. Comparison between experimental data with their 90% confidence intervals (◇) and predicted evolution (—) of the compliance tensor for a 2D SiC–SiC.

account the crack opening displacement and permits a prediction of damage processes such as growing cracks. Moreover, both the influence of the geometry of cracks and the effect of the anisotropy have been illustrated. The introduction of 3D defined transverse cracks leads to a good agreement between experimental data and a prediction for the compliance tensor. The predictions of the non-diagonal compliances remain problematic and point out the necessity to take into account the interaction between cracks with different orientations (Kachanov and Montagut, 1986; Molinari and El Mouden, 1996).

Acknowledgements

C. Barret is grateful to the Région Aquitaine for its partial financial support.

References

Audoin, B., Baste, S., 1994. Ultrasonic evaluation of stiffness tensor changes and associated anisotropic damage in a ceramic matrix composite. J. Appl. Mech. 55, 309–316.

Baste, S., Audoin, B., 1991. On internal variables in anisotropic damage. Eur. J. Mech. A Solids 10, 587–606.

Baste, S., Morgan, J.M., 1996. Under load strain partition of a ceramic matrix composite using an ultrasonic method. Exper. Mech. 36, 148–154.

Bhargava, R.D., Radhakrishna, H.C., 1964. Elliptic inclusion in orthotropic medium. J. Phys. Soc. Japan 19, 396–405.

Budiansky, B., O'Connel, R., 1976. Elastic moduli of a cracked solid. Int. J. Solids Structures 12, 81–97.

Deng, H., Nemat-Nasser, S., 1992. Microcrack arrays in isotropic solids. Mech. Mater. 13, 15–36.

Eshelby, J.D., 1957. The determination of the elastic field of an ellipsoidal inclusion, and related problems. Proc. Roy. Soc. A 241, 376–396.

Evans, A.G., Zok, F.W., 1994. The physics and mechanics of fiber-reinforced brittle matrix composites. J. Mater. Sci. 29, 3857–3896.

Faivre, G., 1971. Hétérogénéités ellipsoïdales dans un milieu élastique anisotrope. J. de Phys. 32, 325–331.

Hashin, Z., 1988. The differential scheme and its applications to cracked materials. J. Mech. Phys. Solids 36, 719–734.

He, M.Y., Wu, B.-X., Evans, A.G., Hutchinson, J.W., 1994. Inelastic strains due to matrix cracking in unidirectional fiber-reinforced composites. Mech. Mater. 18, 213–229.

Hill, R., 1965. A self consistent mechanics of composite materials. J. Mech. Phys. Solids 13, 213–222.

Hoenig, A., 1979. Elastic moduli of a non-randomly cracked body. Int. J. Solids Structures 15, 137–154.

Horii, H., Nemat-Nasser, S., 1983. Overall moduli of solids with microcracks: load-induced anisotropy. J. Mech. Phys. Solids 31, 155–171.

Hosten, B., Baste, S., Choqueuse, D., 1992. Suivi par ultrasons du vieillissement hydrolytique de matériaux composites à matrice organique. In: AMAC (Ed.), Annales des Composites. pp. 65–76.

Kachanov, M., Montagut, E., 1986. Interaction of crack with certain microcrack arrays. Engn Frac. Mech. 25, 625–636.

Laws, N., 1977a. The determination of stress and strain concentrations at an ellipsoidal inclusion in an anisotropic material. J. Elast. 7, 91–97.

Laws, N., 1977b. A note on interaction energies associated with cracks in anisotropic solids. Phil. Mag. 36, 367–372.

Laws, N., 1985. A short note on penny-shaped cracks in transversely isotropic materials. Mech. Mater. 4, 209–212.

Laws, N., Dvorak, G.J., 1987. The effect of fiber breaks and aligned penny-shaped cracks on the stiffness and energy release rates in unidirectional composites. Int. J. Solids Struct. 23, 1269–1283.

McLaughlin, R., 1977. A study of the differential scheme for composite materials. Int. J. Engng Sci. 15, 237–244.

Molinari, A., El Mouden, M., 1996. The problem of elastic inclusions at finite concentration. Int. J. Solids Structures 33, 3131–3150.

Mori, T., Tanaka, K., 1973. Average stress in matrix and average energy of materials with misfitting inclusions. Acta Metal. 21, 571–574.

Morvan, J.-M., Baste, S., 1998. Effect of two-scale transverse cracks systems on the non linear behaviour of a 2D SiC–SiC composite. Mater. Sci. Eng./A., A250, 231–240.

Wang, S.S., Chim, E.S.-M., Suemasu, H., 1986. Mechanics of fatigue damage and degradation in random short-fiber composites, Part II—Analysis of anisotropic property degradation. ASME J. Appl. Mech. 53, 347–353.

Willis, J.R., 1964. Anisotropic elastic inclusion problems. Quart. J. Mech. Appl. Math. 17, 157–174.

Zaoui, A., 1996. Méthodes de changement d'échelle en micromécanique des composites. In: AMAC (Ed.), Proceeding of JNC10. pp. 13–26.

Zhao, Y.H., Tandon, G.P., Weng, G.J., 1989. Elastic moduli for a class of porous materials. Acta Mech. 76, 105–130.